

DESY SR-82-22
December 1982

DETERMINATION OF PARTIAL SUBSHELL CROSS-SECTIONS AND ELECTRON MEAN FREE
PATH IN SOLIDS WITH THE PHOTOEMISSION SET-UP AT THE FLIPPER MONOCHROMATOR

by

J. Barth, F. Gerken and C. Kunz

*II. Institut für Exp.-Physik, Universität Hamburg
and HASYLAB at Deutsches Elektronen-Synchrotron DESY, Hamburg*

Eigentum der	DESY	Bibliothek
Property of		library
Zugang:	8. FEB. 1983	
Accessions:		
Leihfrist:	7	Tage
Loan period:		days

ISSN 0723-7979

NOTKESTRASSE 85 · 2 HAMBURG 52

DESY behält sich alle Rechte für den Fall der Schutzrechtserteilung und für die wirtschaftliche Verwertung der in diesem Bericht enthaltenen Informationen vor.

DESY reserves all rights for commercial use of information included in this report, especially in case of filing application for or grant of patents.

To be sure that your preprints are promptly included in the
HIGH ENERGY PHYSICS INDEX ,
send them to the following address (if possible by air mail) :

DESY
Bibliothek
Notkestrasse 85
2 Hamburg 52
Germany

DETERMINATION OF PARTIAL SUBSHELL CROSS-SECTIONS AND ELECTRON MEAN FREE
PATH IN SOLIDS WITH THE PHOTOEMISSION SET-UP AT THE FLIPPER MONOCHROMATOR

J. Barth, F. Gerken and C. Kunz

II, Institut f. Exp.-Physik, Universität Hamburg, 2000 Hamburg 52
and HASYLAB at DESY, 2000 Hamburg 52, FRG

The methods of quantitative measurements of photoemission intensities on solids are outlined for experiments using monochromatized synchrotron radiation as a tunable light source. Results are explicitly calculated for the photoemission set-up at the FLIPPER monochromator which covers the energy range between 20 eV and 500 eV. A procedure is given to determine the transmission of an electron analyzer in the retarding mode.

to be published in: Proceedings of the International Conference on X-Ray and VUV Synchrotron Radiation Instrumentation, Hamburg, August 1982, Nucl. Instr. & Methods in Physics Research.

The photoemission intensity of a subshell excited in a solid is determined by both the excitation probability and the probability for the photoelectron to leave the solid without being scattered inelastically. Thus the measurement of partial cross-sections of atoms in the solid state and of the mean free path of the photoelectrons are closely related, both of them being of fundamental value. To extract these quantities from measurements of photoemission intensities the excitation and escape probabilities have to be calculated. For this purpose the 3-step-model of Berglund and Spicer¹ is a very practical approximation to the photoemission process in the solid. Fadley has listed up a number of additional assumptions which simplify calculations for idealized systems².

Experimentally, the detection probability of the photoelectrons by the electron analyzer has to be determined. Palmberg studied a commercial double pass cylindrical mirror analyzer (CMA) which is commonly used for angular integrated measurements³. However, the theoretically expected transmission of a CMA in the retarding mode (i.e. at constant resolution) could not be verified in the experiment³. Still it was used as an approximation in many partial subshell cross-section measurements which were performed on non-transition metals⁴ and transition metals with the particularly interesting manifestations of intershell interactions⁵. The escape probability was considered only in a very recent study of the 4f cross-section of Au by Johansson et al⁶. Alternatively, Hecht and Lindau determined the cross-sections of Ba and operating the CMA in the normal mode (i.e. without retarding voltage), where the transmission varies as the resolution of the CMA⁷. However,

for many purposes it is essential to independently choose the resolution of a CMA which is only possible in the retarding mode.

It is the purpose of this paper to present a new practical method to determine the transmission of a CMA in the retard mode as a function of the ratio between kinetic and pass energy. Furthermore, starting from the 3-step-model and common assumptions for an idealized solid surface, we derive an expression for the escape probability of the photoelectrons. This allows an evaluation of the photoelectron mean free path and partial subshell cross-section from photoemission intensities if the core level binding energies are shifted at the surface ("surface shift"). In this case, bulk and surface photoemission can be distinguished energetically and the mean free path may be extracted from the bulk-to surface intensity ratio, since only the bulk emission is influenced by inelastic scattering.

The photoemission intensity of a subshell as measured must be corrected for the photon flux of the monochromator and the transmission of the analyzer. At the FLIPPER monochromator the photon flux is obtained by a photodiode that can be moved into the beam behind the exit slit⁸ (see Fig. 1). Different from gas phase measurements the source volume from which a CMA accepts electrons is not the same for each measurement, but depends on the sample adjustment. It is given by the intersection between the source volume, the sample surface and the light spot. In addition, the CMA acceptance area on the surface varies as a function of the ratio between E_{kin} and E_{pass} , theoretically the area

is predicted to be proportional to $(E_{kin}/E_{pass})^{-1}$.³ In the experiment E_{kin} is tuned. However, to determine the CMA transmission, we follow the intensity variation at fixed E_{kin} tuning E_{pass} for the same geometrical conditions. Because photon energy and kinetic energy are fixed the intensity variation is now only a function of the analyzer transmission. Dividing this measured intensity by E_{pass} accounts for the variation due to the change in the CMA resolution. The corrected intensity plotted versus E_{kin}/E_{pass} gives the CMA transmission (Fig. 2). A change in E_{kin} by a factor of 3 leaves the result unchanged within 5 % except for values of E_{pass} below 5 eV where residual fields in the CMA are expected to disturb the electrons' trajectories. Above this value, however, the result shows that the analyzer transmission is in fact a function only of the ratio between kinetic and pass energy. Large deviations from the predicted behaviour proportional to $(E_{kin}/E_{pass})^{-1}$ occur when the CMA acceptance area and the light spot only partly overlap for small values of E_{kin}/E_{pass} . The arrow in Fig. 2 marks the minimum ratio where the CMA acceptance area is completely inside the light spot. This is determined by the image of an aperture inside the CMA which is projected onto the sample by the retarding grids³.

We now turn to the calculation of photoemission intensities. The number of photoelectrons per time interval which leave the solid sample without being scattered inelastically is determined by:

$$N_e(\hbar\omega, E) = \int_x \int_{\Omega} N_{Ph}(\hbar\omega, x) p_{ex}(\hbar\omega, E, \Omega) dx d\Omega p_{es}(E, x, \Omega) p_{de}(E, \Omega) \Delta E \quad (1)$$

Here, N_{ph} denotes the number of photons impinging on the surface per time interval, p_{ex} the excitation probability per depth element dx and solid angle element $d\Omega$, p_{es} the escape probability, and p_{de} the detection probability per energy resolution interval ΔE . Further, the kinetic energy is simply written as E , and x stands for the distance from the surface which is assumed to be atomically flat.

The detection probability can be split into the analyzer transmission $t(E/E_{pass})$ which is independent of Ω , and the angular acceptance $g(\Omega)$. This is justified if the dimensions of the effective probing area are small compared to its distance from the CMA. Making also use of the proportionality between the CMA resolution and the pass energy we write:

$$p_{de}(E, \Omega) = g(\Omega) \cdot t(E/E_{pass}) C_0 E_{pass} \quad (2)$$

where C_0 is a constant.

Since in the energy region of interest the absorption length is much larger than the photoelectron attenuation length, the number of photons reaching the depth x can be approximated by the number of photons impinging on the surface. Therefore, photon flux, analyzer transmission and pass energy can be used to correct the measured photoemission intensity:

$$I_{corr} = \frac{N_e(h\nu, E)}{N_{ph}(h\nu) t(E/E_{pass}) C_0 E_{pass}} = \int_x \int_{\Omega} p_{ex}(h\nu, E, \Omega) p_{es}(E, x, \Omega) g(\Omega) dx d\Omega \quad (3)$$

For the variables that determine Ω it is essential to define whether they are measured inside or outside the sample. Both sets of variables can be transformed into each other using the conditions for the surface refraction. If we choose the surface normal of the sample as the polar axis we can express Ω in polar coordinates, and the transformation between the angles inside (ϕ' , θ') and outside the sample (ϕ , θ) is given by $\phi' = \phi$; $\frac{\sin \theta'}{\sin \theta} = \sqrt{\frac{\epsilon - 1}{\epsilon}}$; $\epsilon = \frac{E_{kin} + V_0}{V_0}$, with V_0 being the inner potential of the sample. Since in eqn. (3) the functions p_{ex} and p_{es} are determined inside the sample it is convenient to write the integral in terms of θ' and ϕ' :

$$I_{corr} = \int_x \int_{\theta'} \int_{\phi'} p_{ex}(\theta', \phi') p_{es}(x, \theta') g(\theta', \phi') \sin \theta' dx d\theta' d\phi' \quad (3a)$$

where we have used the same functional symbols inside and outside. For simplicity we have also omitted the energy variables.

The excitation probability is linked to the essentially atomic quantities of the photoionization cross-section σ and the asymmetry parameter β :

$$p_{ex} = \rho \frac{\sigma}{4\pi} (1 + \beta P_2(\cos \delta')) \quad (4)$$

The angle δ' is measured between the electric vector of the radiation and the direction of the outgoing photoelectron, ρ denotes the atomic density and P_2 is the Legendre polynom. The escape probability contains the characteristics of the solid namely the mean free path λ and the topology of the surface which for simplicity is again assumed to be flat:

$$p_{es} = \exp\left(-\frac{x}{\lambda \cos \theta'}\right) \text{ with } \theta' \leq \theta_{\max} \quad (5).$$

Surface refraction limits the range of θ' for which the electrons can penetrate through the surface. This effect is automatically accounted for if we now transform eqn. (3a) to the angles measured outside the sample. Neglecting an angular asymmetry of the photoelectrons we carry out the ϕ -integration over the angular acceptance function

$$\int_0^{2\pi} g(\theta, \phi) d\phi = 2\pi f(\theta),$$

and arrive at the following expression for the photoemission intensity

$$I_{\text{corr}} = \frac{\rho^3}{2} \sqrt{\frac{\epsilon-1}{\epsilon}} \int_0^{\infty} \int_0^{\pi/2} \exp\left(-\frac{x}{\lambda \sqrt{\frac{\epsilon-1}{\epsilon}} \sqrt{\cos^2 \theta + \frac{1}{\epsilon-1}}}\right) f(\theta) \sin \theta dx d\theta \quad (6)$$

The total photoemission intensity of a subshell nl is not the only information accessible to experiments. Angle resolved measurements and measurements of only the surface emission intensity yield a complete data set to determine all parameters that influence photoemission intensities. The relation between these sample properties and the measurable intensities is sketched in Fig. 3. From the left to the right, each experiment depicted in Fig. 3 requires the information of the former. In an angle resolved measurement of the bulk-to-surface intensity ratio taken at different polar angles θ with respect to the surface normal, the mean free path stays constant for constant excitation energy. Thus such an experiment may be suited to determine the surface topology. When the escape probability is matched to this result, measurements at varying excitation

energies yield the mean free path. These measurements are much easier carried out using an angle integrating analyzer with the advantage of much higher count rates. Likewise the asymmetry parameter and the partial subshell cross-section may be extracted from total photoemission intensities in angle resolved and angle integrated measurements.

Angle resolved measurements of bulk-to-surface intensity ratios require an extremely high photon flux at high resolution so that these experiments appear not to be feasible at present. Only one experiment of this type was reported for evaporated Au by use of an X-ray source⁹. The data show evidence for surface roughness⁹ so that in principle this type of measurements may be exploited to study surface roughnesses on a microscopic scale. A detailed analysis of these effects on angle integrated measurements of the bulk-to-surface intensity ratio showed that the influence is lower than the experimental error¹⁰. This justifies the assumption of an atomically flat surface for these types of experiments.

The bulk-to-surface intensity ratio is then calculated using equation (5) only for the bulk emission and omitting the inelastic attenuation for the surface emission. If the excitation probability is independent of x and θ it may be taken out of the integral. These assumptions are justified since the absorption length is much larger than the photoelectron attenuation length and if the influence of the atomic asymmetry parameter β may be neglected, e.g. because the CMA axis and the electric vector of the radiation include the "magic angle" of $54^\circ 44'$. Now the angular acceptance of the CMA is needed. For the FLIPPER experiment the geometry of the sample and the CMA is shown in Fig. 4. The synchrotron radiation is polarized in the x - y plane against which the CMA axis is tilted by 45° . In this case, an extreme

variation of β changes the total intensity by -8% and +16%. Surface refraction lowers this intensity variation even further so that it may well be neglected. The angular acceptance $f(\theta)$ calculated for different sample adjustments is plotted versus the polar angle θ in Fig. 5.

According to Fig. 3 the bulk-to-surface intensity ratio is calculated by integrating the escape probabilities, multiplied with the analyzer angular acceptance, over x and Ω :

$$\frac{I_B}{I_S} = \frac{\rho_B \int_a^\infty \int_\Omega P_{eS} g(\Omega) d\Omega dx}{\rho_S \int_0^a \int_\Omega g(\Omega) d\Omega dx}$$

$$= \frac{\rho_B \lambda \sqrt{\frac{\epsilon-1}{\epsilon}}}{\rho_S \frac{\lambda}{a} \sqrt{\frac{\epsilon-1}{\epsilon}}} \frac{\int_0^{\pi/2} f(\theta) \sin\theta \sqrt{\cos^2\theta + \frac{1}{\epsilon-1}} \exp\left(-\frac{a}{\lambda \sqrt{\frac{\epsilon-1}{\epsilon} \sqrt{\cos^2\theta + \frac{1}{\epsilon-1}}}}\right) d\theta}{\int_0^{\pi/2} f(\theta) \sin\theta d\theta}$$

Here, a denotes the thickness of a surface layer. Fig. 6 shows the intensity ratios versus the mean free path with ϵ as a parameter. The angular acceptance $f(\theta)$ used here corresponds to the geometry of the FLIPPER experiment with a sample adjustment of $\alpha = 30^\circ$ (see Fig. 4).

As an example for the experimental determination of the mean free path from bulk-to-surface intensity ratios Fig. 7 shows our measurements on evaporated Au together with the corresponding fits for the bulk and surface emission. Our fitting procedure is described in Ref. 11. From experiments on well defined single crystal surfaces we know the position and relative intensities of the surface shifted core levels for the low index surface orientations¹². Our spectra of the evaporated Au film can be fitted using

both a (111)- and (110)-surface component which show the same surface shift¹², and a (100)-surface component which can be distinguished from the others¹². The (100)-contribution may only be varied between 20% and 50% to obtain reasonable fits to our data. Assuming a 33% contribution for each low index surface we are left with the bulk-to-surface intensity ratio as the only adjustable parameter since the lineshape parameters are known from bulk sensitive XPS measurements (see Ref. 9), and the atomic density at the surface can be taken from the experiment on the single crystals reported in Ref. 12. By use of Fig. 6 the mean free path is easily determined, the result is shown in Fig. 8 ($a_{Au} = 2.2 \text{ \AA}^9$). We estimate the error of this method of a mean free path determination to be 30% which makes it superior to other methods in this energy range.

The excitation probability of core levels is dominated by atomic properties. Even the asymmetry parameter β maintains its importance in the solid as angle resolved measurements revealed¹³. Here again we focus on angle integrated measurements neglecting the angular asymmetry for the reason given above. According to eqn. (6) the total intensity of a subshell n_l can be written as:

$$I_{n_l} = \frac{\sigma_{n_l}}{2} \rho \frac{\epsilon-1}{\epsilon} \lambda \int_0^{\pi/2} \sqrt{\cos^2\theta + \frac{1}{\epsilon-1}} f(\theta) \sin\theta d\theta$$

$$= \rho \sigma_{n_l} \lambda K$$

This defines the correction function K which is shown in Fig. 9 (for the geometry of the FLIPPER experiment). The product of $\lambda \cdot K$ contains all solid state corrections to the total photoemission intensity. For Au we have interpolated the mean free path λ using our data and those of Kanter¹⁴ for lower energies (see Fig. 8). The resulting product $\lambda \cdot K$ for Au is shown in Fig. 10.

Our result indicates that the total photoemission intensity is strongly influenced by solid state corrections in the energy range below the minimum of the mean free path, less affected, however, above the minimum of the mean free path. This is due to the moderate variation of both the emission cone caused by surface refraction (compare Fig. 9) and the mean free path (compare Fig. 8) in this energy range. This allows partial cross-section determinations without detailed knowledge of the mean free path. The situation is illustrated by the analysis of the mean free paths in the rare earth metals Eu and Gd and the 4f cross-section of Gd. The surface shift of these materials has been described previously together with a less detailed analysis of the mean free path¹¹. The measurements on these materials have been continued with even enhanced resolution¹⁶. The resulting mean free path evaluated with help of Fig. 6 is displayed in the upper part of Fig. 11. Since no data on single crystals are available we assume that the density of atoms in the surface layer is equal to that of a bulk layer of the same thickness. The mean free path of both materials can be fitted by a single curve, for simplicity we approximate it by a straight line. The lower part of Fig. 11 shows the 4f intensity both with and without the solid state correction $\epsilon \cdot K$. This curve contains the dramatic 4d-4f resonance around 150 eV photon energy¹⁷. We want to stress that the lineshape of this resonance even over a wider energy range is nearly unaffected by the solid state correction.

However, if cross-section measurements cover the energy range below the minimum of the mean free path the solid state corrections to the photoemission intensity are of crucial importance. In this context we note that in a previous study of the 4f cross-section of solid Au, Johansson et al⁶ were left with a discrepancy of an order of magnitude between the results determined by the direct 4f-photoemission intensity and the results determined by the N00 (4f 5d 5d)-Auger intensity near threshold. For energies higher than 100 eV above threshold, both results matched. The discrepancy was attributed to the effect of higher order light from the monochromator⁶. Based on our results we can easily add further explanations of this discrepancy: the transmission of the CMA deviates from the theoretically predicted behaviour in the low energy region (see Fig. 1); the mean free path used by Johansson et al is based on less exact determinations and shows a wrong energy dependence below 100 eV kinetic energy. This stresses the importance of both the determination of an analyzer's transmission function and of the combined theory for the calculation of bulk-to-surface intensity ratios and total photoemission intensities.

We thank R. Nyholm for a critical reading of the manuscript.

This work was supported by Bundesministerium für Forschung und Technologie BMFT from Funds for Research with Synchrotron Radiation.

References

- 1) C.N. Berglund and W.E. Spicer, Phys. Rev. A 136, 1030 (1964)
- 2) C.S. Fadley, J. Electr. Spectr. Relat. Phenom. 5, 725 (1974)
- 3) P.W. Palmberg, J. Electr. Spectr. Relat. Phenom. 5, 691 (1974), and J. Vac. Sci. Techn. 12, 379 (1975)
- 4) L.I. Johansson, I. Lindau, M.H. Hecht, S.M. Goldberg and C.S. Fadley, Phys. Rev. B 20, 4126 (1979)
- 5) J. Barth, F. Gerken, K.L.I. Kobayashi, J.H. Weaver and B. Sonntag, J. Phys. C 13, 1369 (1980)
- 6) L.I. Johansson, M.H. Hecht and I. Lindau, J. Electr. Spectr. Relat. Phenom. 18, 271 (1980)
- 7) M.H. Hecht and I. Lindau, Phys. Rev. Lett. 47, 821 (1981)
- 8) J. Barth, F. Gerken, J. Schmidt-May and C. Kunz, this conference accompanying paper
- 9) P.H. Citrin, G.K. Wertheim and Y. Baer, Phys. Rev. Lett. 41, 1425 (1978)
- 10) J. Barth, thesis University of Hamburg (in preparation)
- 11) R. Kammerer, J. Barth, F. Gerken, A. Flodström and L.I. Johansson, Solid State Commun. 41, 435 (1982)
- 12) P. Heimann, J.F. van der Veen and D.E. Eastman, Solid State Commun. 38, 595 (1981)
- 13) R.F. Davis, S.D. Kevan, B.-C. Lu, J.G. Tobin and D.A. Shirley, Chem. Phys. Lett. 71, 448 (1980)
- 14) H. Kanter, Phys. Rev. B 1, 522 (1970)
- 15) J. Szajman and R.C.G. Leckey, J. Electr. Spectr. Relat. Phenom. 23, 83 (1981)
- 16) F. Gerken, thesis University of Hamburg (in preparation)
- 17) F. Gerken, J. Barth and C. Kunz, X-Ray conference, Eugene 1982, invited paper, to be published in the AIP conference series.

Figure Captions

- Fig. 1 Revolving photodiode that can be moved into the photon beam behind the exit slit of the monochromator. Two cathodes may be used alternatively.
- Fig. 2 Transmission function of a CMA experimentally determined for one particular sample adjustment at two different kinetic energies. The theoretically predicted behaviour is shown by the solid line.
- Fig. 3 Connection between sample properties and measurable photoemission intensities. The symbols are explained in the text.
- Fig. 4 Collection geometry of the CMA at the FLIPPER experiment. The analyzer axis is in the y-z plane tilted by 45° against the z-axis. The sample surface normal n is in the z-x plane tilted by the angle α against the z-axis. As shown the sample is excited in s-polarization. P-polarization is reached by turning the surface normal n into the x-y plane. This leaves the collection geometry unchanged.
- Fig. 5 Analyzer acceptance for the collection geometry of Figure 4, calculated for different angles α .
- Fig. 6 Bulk-to-surface photoemission intensity ratios versus the mean free path calculated for different values of ϵ using the angular acceptance for $\alpha = 30^\circ$.
- Fig. 7 Energy distribution curves for the $4f_{7/2}$ photoelectrons from evaporated Au (overall resolution 0.1eV) and corresponding fits for bulk and surface emission as described in Ref. 11. The decomposed bulk and surface contributions are shown for the 170eV-spectrum.
- Fig. 8 Mean free path for evaporated Au determined from the bulk-to-surface intensity ratios with help of Fig. 6. The values below 11 eV are taken from Ref. 14, the theoretical curve from Ref. 15.
- Fig. 9 Correction function K for the total photoemission intensity (see text).
- Fig. 10 Solid state correction $\epsilon \cdot K$ for the total photoemission intensity of evaporated Au (see text).
- Fig. 11 Mean free path for evaporated Eu and Gd (upper panel) and $4f$ cross-section of Gd.

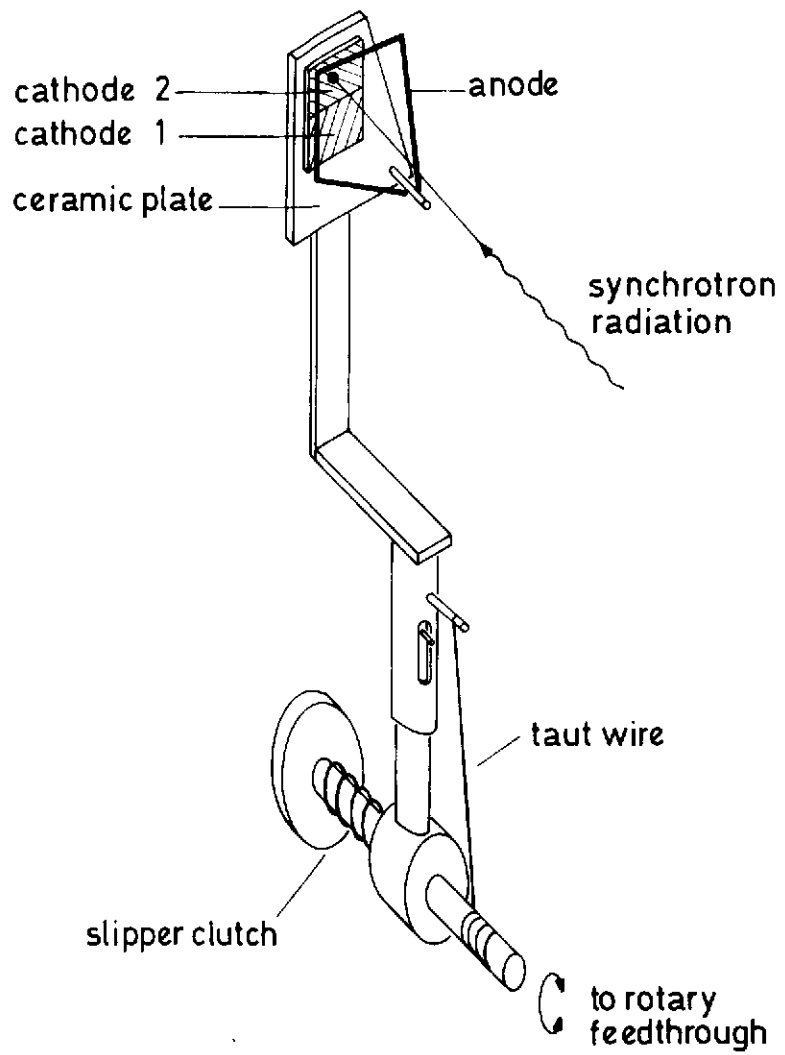
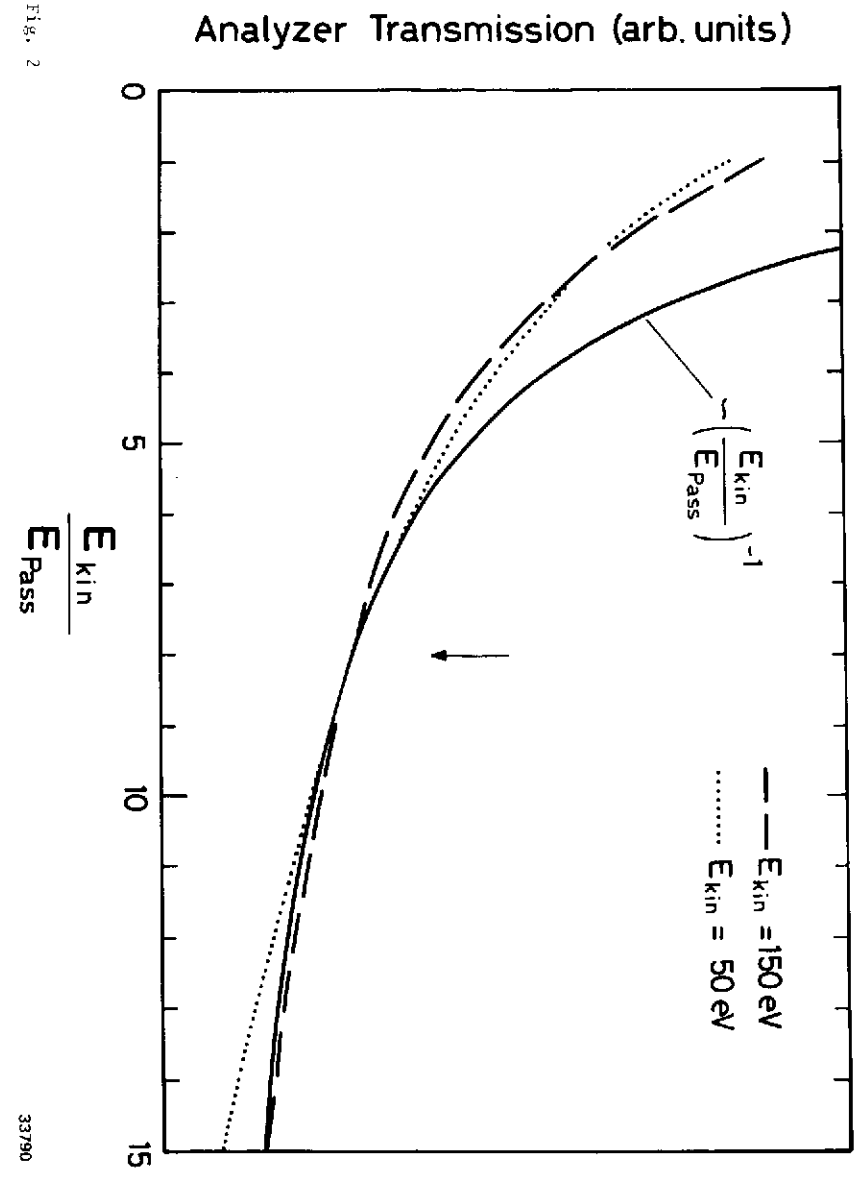


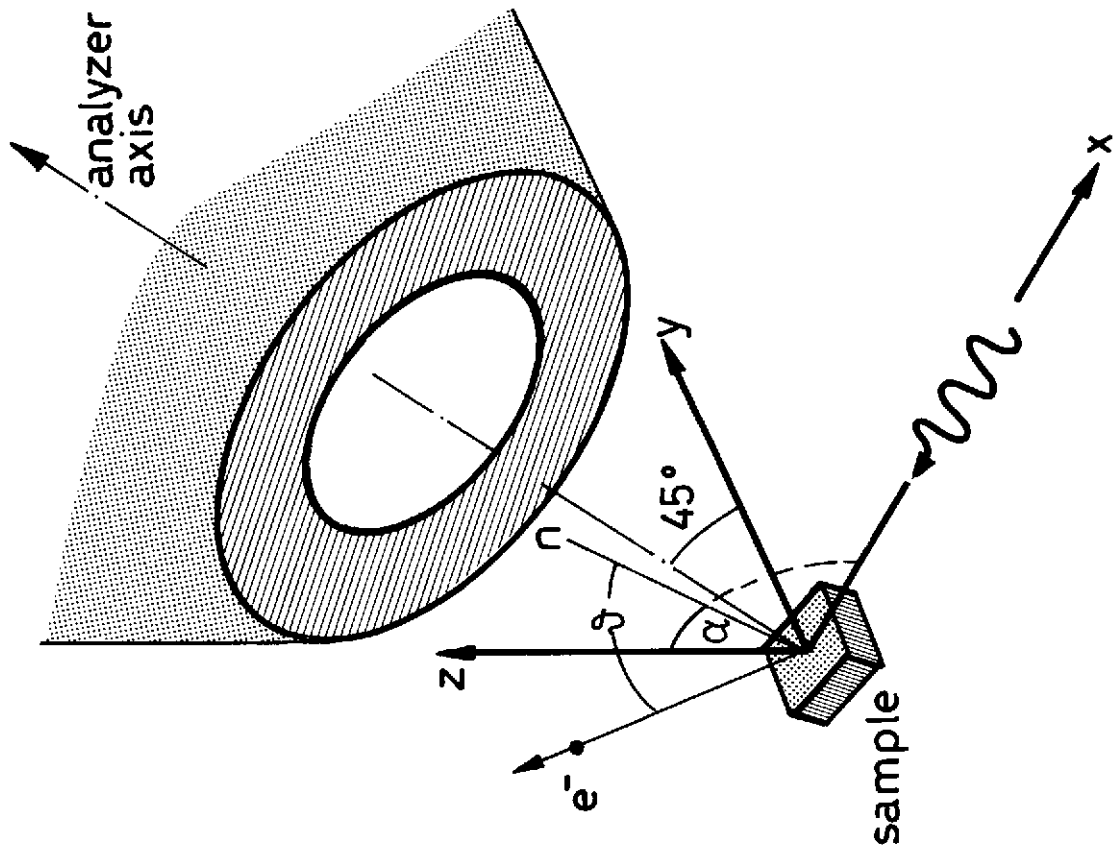
Fig. 1

34095

Fig. 2

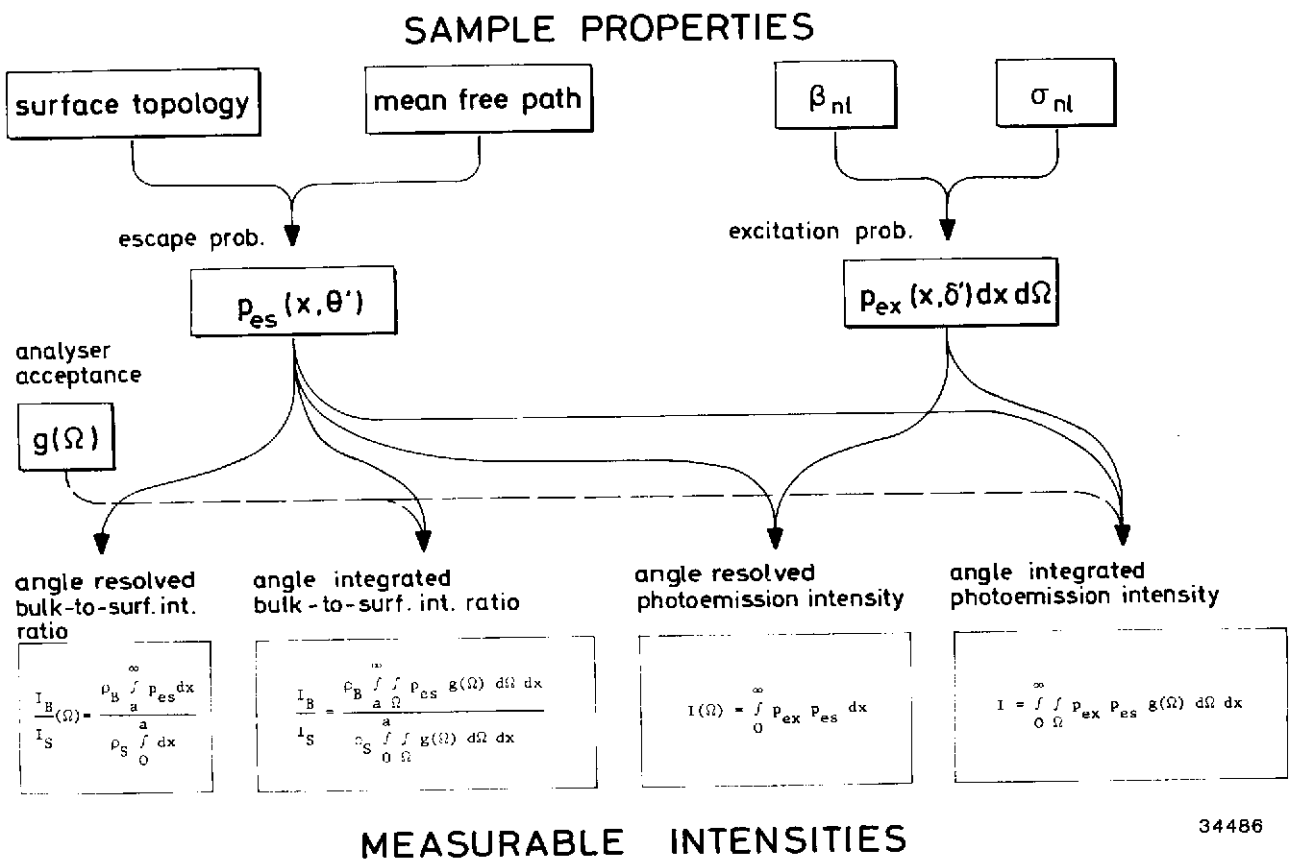


33790



34276

Fig. 4



34486

Fig. 3

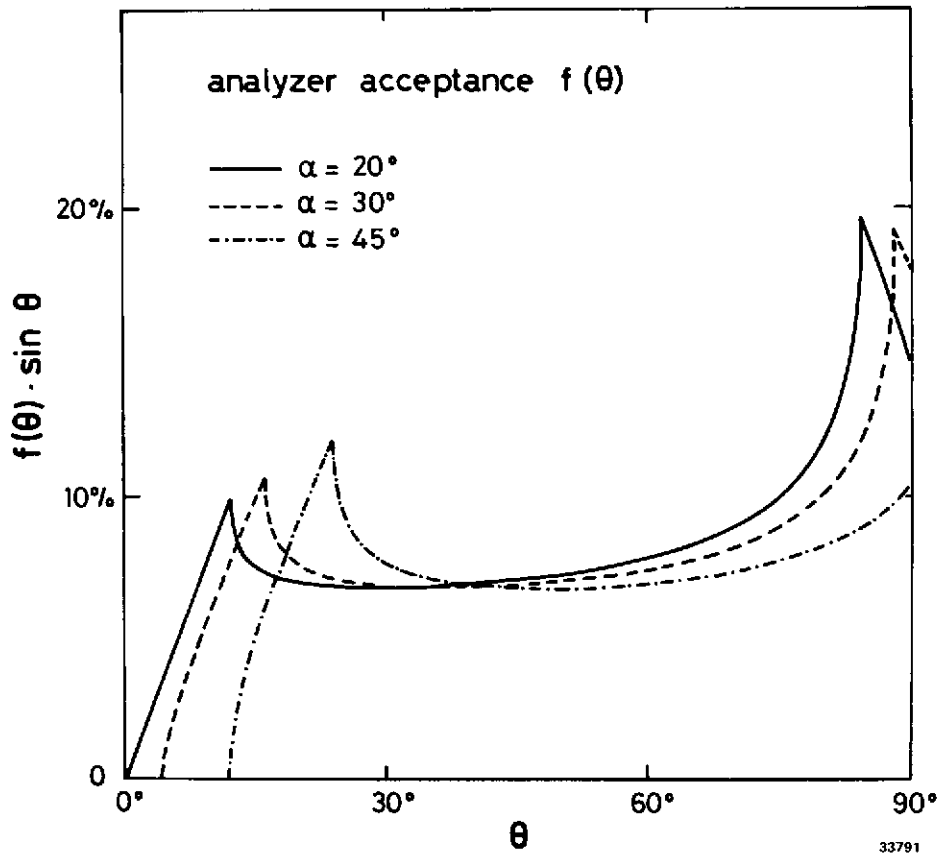


Fig. 5

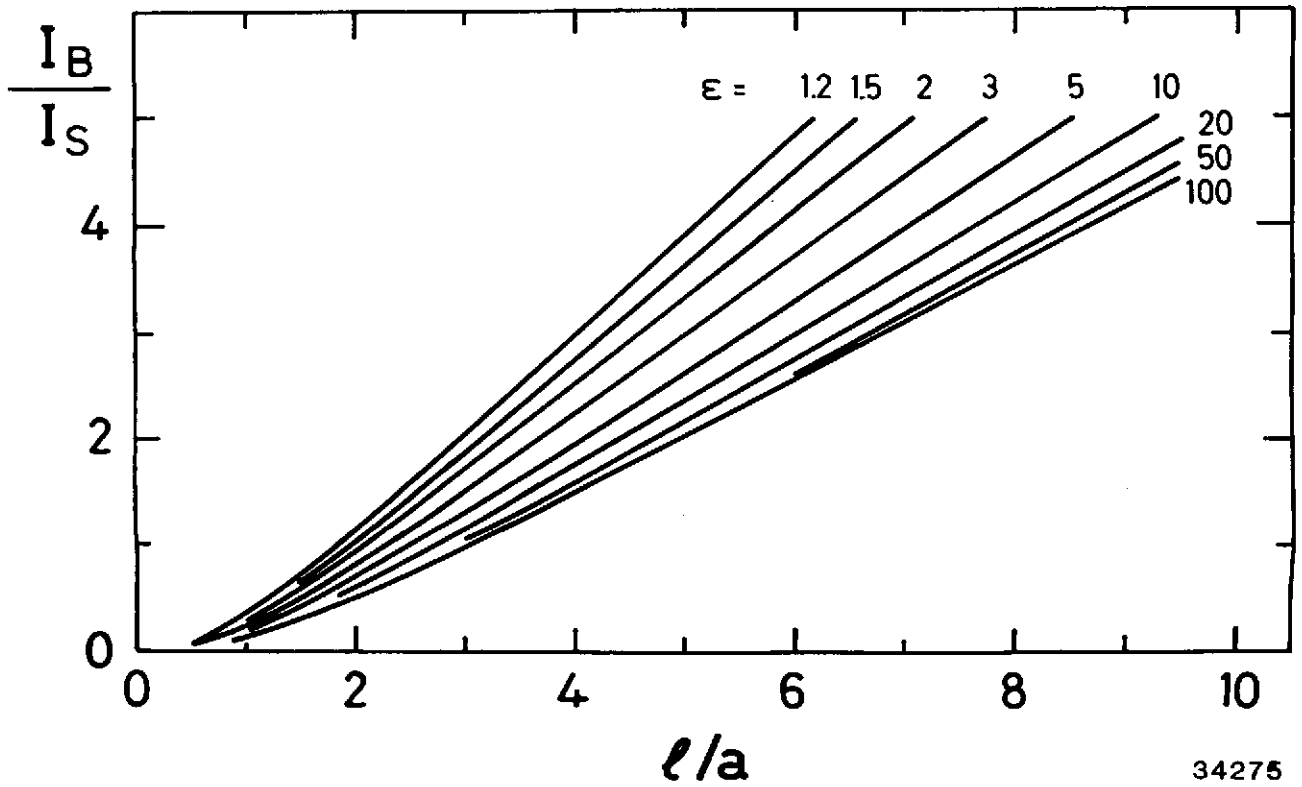


Fig. 6

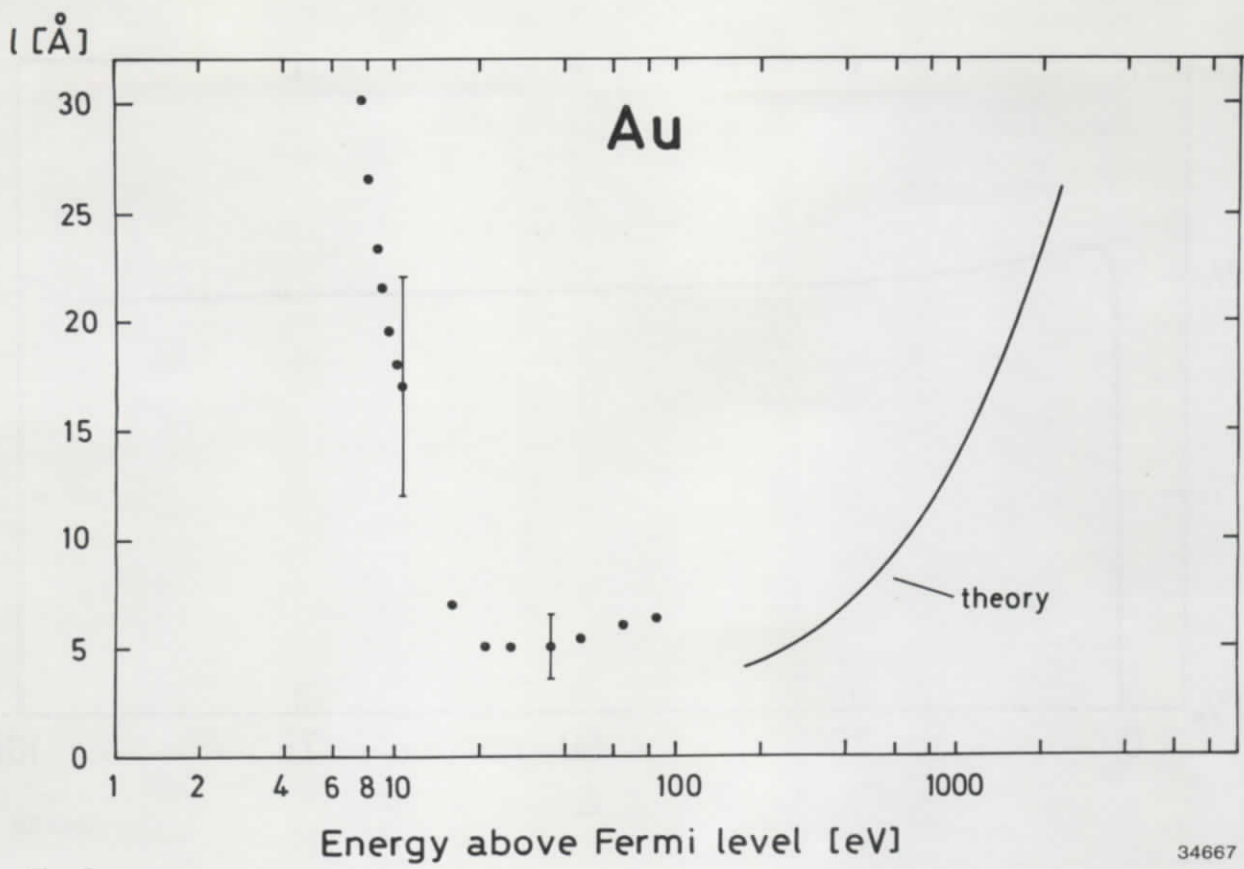


Fig. 8

34667

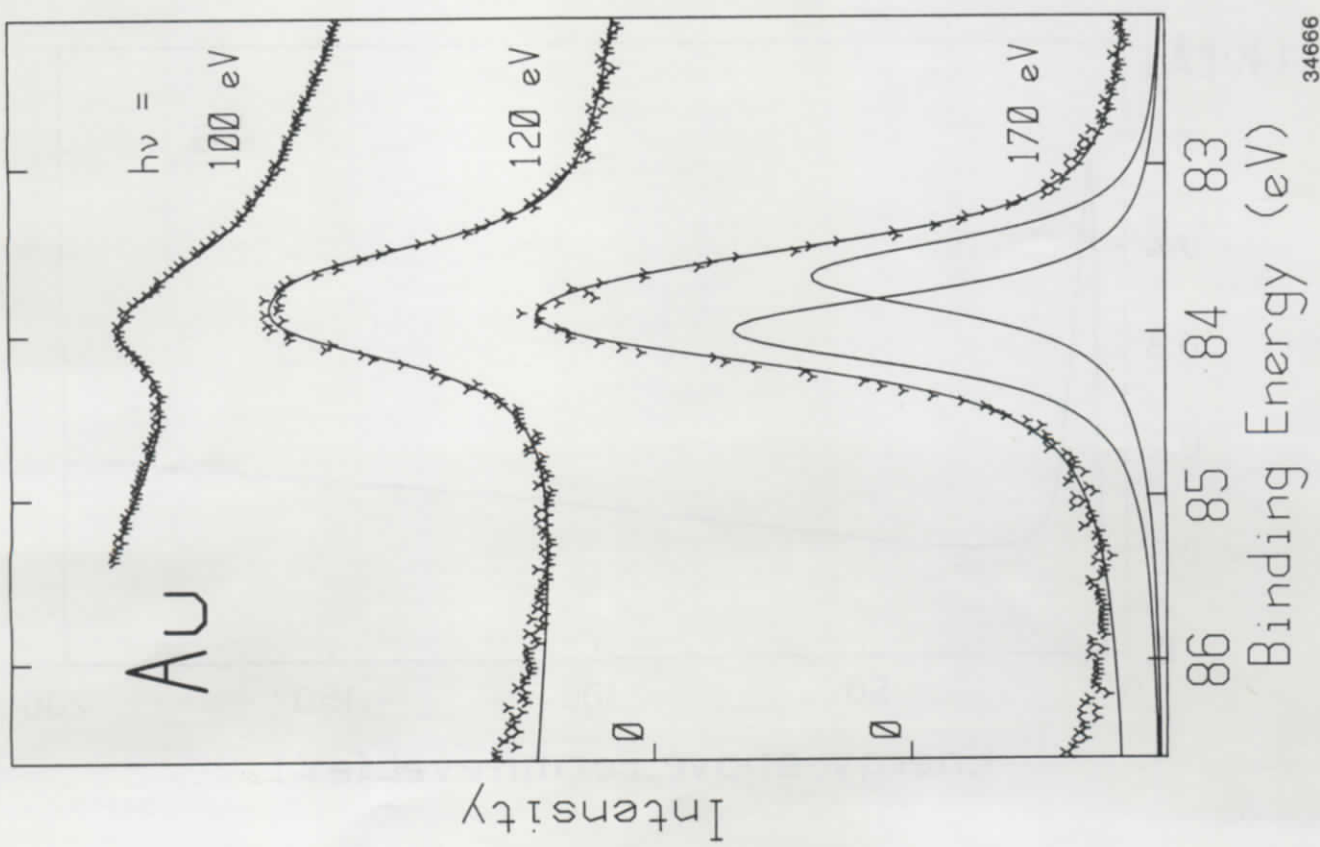


Fig. 7

34666

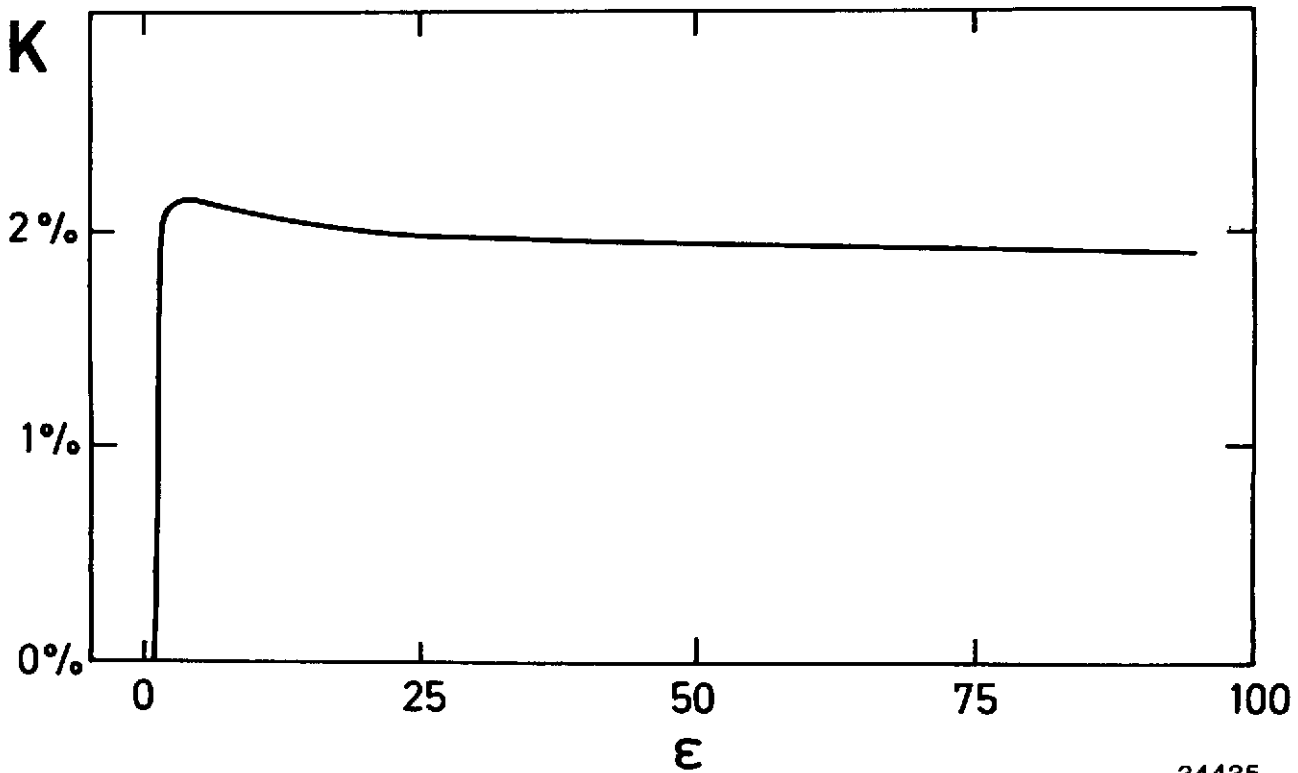


Fig. 9

34435

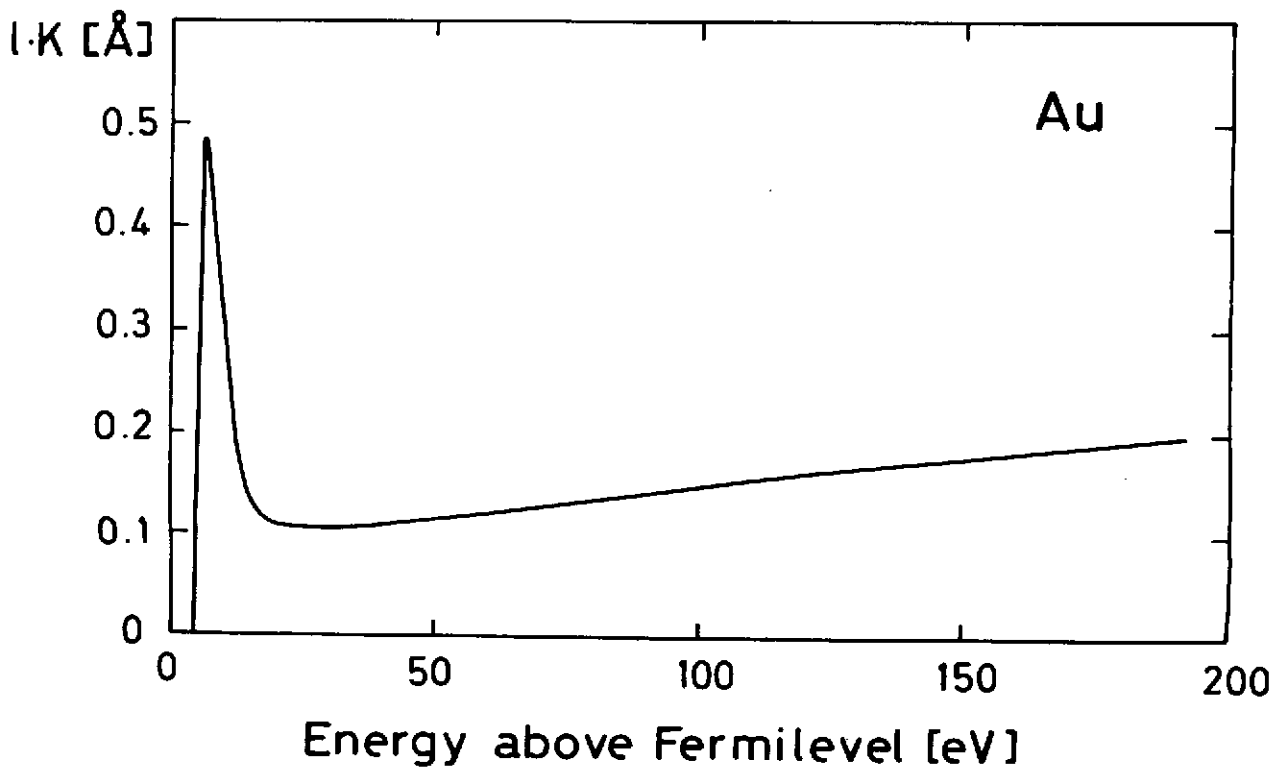


Fig. 10

34272

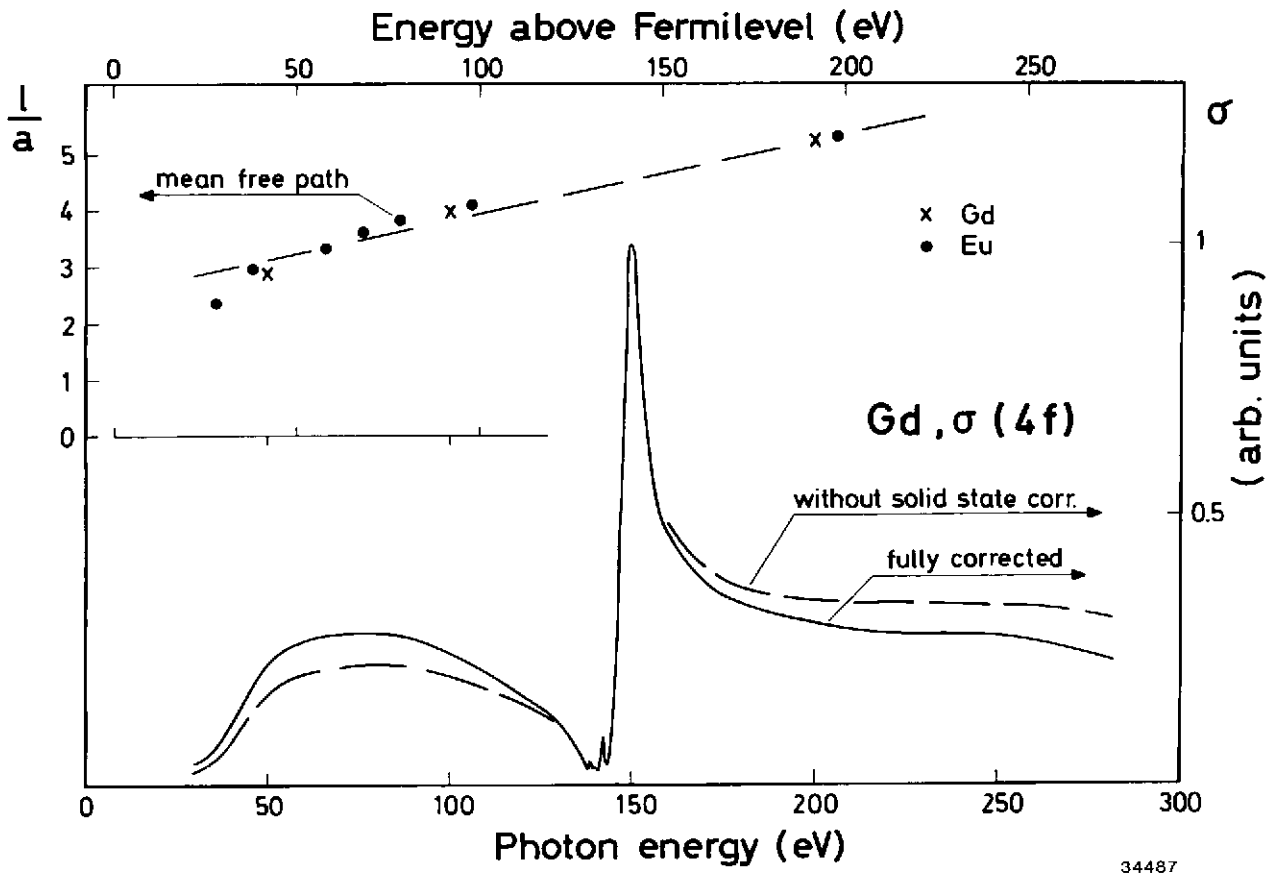


Fig. 11

34487

